# Chapter 6

# Geophysical flows

Geophysical turbulence in the oceans and in the atmosphere is usually non homogeneous and non stationary in nature. These flows play an important role in environmental research both for their intrinsic physical interest and because their practical applications. The subject of geophysical turbulence has tended to focus on the dynamics of large-scale motions in the atmosphere and the oceans. It is on large scales that the common character of atmospheric and oceanic dynamics is most evident, while at the same time the nature of currents like the Gulf Stream in the ocean and the atmospheric jet stream makes such a focus of attention worthwhile. Here, however, we will concentrate on small-scale flows.

The statistical and scaling properties of geophysical flows have been analyzed in considerable detail, but many phenomena are not completely understood, such as intermittency, which sustains the interest in such flows. Most of the current theories invoke homogeneity and isotropy, which are rarely encountered. Moreover, geophysical data possess some uncertainties because the flows are not well controlled and forcing occurs at many scales. In many real systems, there are two important anomalies: deviation from Gaussian distribution on large scales and deviation from local homogeneity, isotropy and stationarity (Babiano *el al.* (1995, 1997)). A very important geophysically driven non-homogeneous turbulent flow is that generated by breaking waves in the surf-zone.

In this chapter, we present a detailed investigation of the statistical and scaling properties of small-scale oceanic velocity data collected in two different locations: in the Ebro Delta (Spain) and in Knebel Vig bay (Denmark). The velocity time series measurements were carried out using an acoustic Doppler velocimeter SONTEK-3D and a 2D Electro-magnetic sensor (EMS), wich will be described in this chapter. Long time series of velocity measurements have been analyzed using the power spectra and the probability distribution functions PDFs to examine the characteristics of the inertial subrange, and the effects of non-homogeneity and intermittency.

Extended Self Similarity (ESS) was used to determine the relative scaling exponents $\zeta_p/\zeta_3$. The influence of the large scale non-homogeneity of wave-wind motion and breaking waves on the scaling properties of the longitudinal velocity structure functions are also investigated.

## 6.1 Experimental setup

As mentioned above, the velocity data were measured using two different sensors: 2D Electro-magnetic current meters, Delft Hydraulics p-S type (figure 6.1) described in detail in Rodriguez (1997), and an acoustic Doppler velocimeter SONTEK-3D, described in chapter 4. The first sensor was used in the Ebro Delta, on the Mediterranean, located on the Spanish coast, 200 Km southwest of Barcelona (figure 6.2). One hour time series of the two components of horizontal velocity were sampled at 20 Hz. A distribution of 6 EMS in depth was used to investigate the non-homogeneity of the turbulence in depth. The vertical spacing of EMS range was 0.2 m, starting at 0.1 m above the sea-bottom and up to 1.4 m above the sea-bottom. The measurements were performed at different non dimensional distances from bottom $Z/d$, where $Z$ is the distance between sensor and bottom, while $d$ is the average depth at the measuring site. In this chapter, only the non-dimensional distances from the bottom $Z/d = 0.8$ and $Z/d = 0.07$ are analyzed.

Figure 6.1: The 2D Electro-magnetic current meters.

The measured velocity data were first filtered by removing spurious spikes after the 2D values had been projected into cross-shore $u$ and long-shore $v$ components using the compass and the topographic surveys, see Rodriguez *et al.* (1999) for further information. Only data that passed the quality control criteria (Yelland and Taylor, (1996)) were taken into account. We have investigated the most energetic day 27 November, 1996, in order to ensure that the Reynolds number is large enough and to study the influence of the non-homogeneity and non-isotropy on the scaling laws as a function of distance from the bottom.

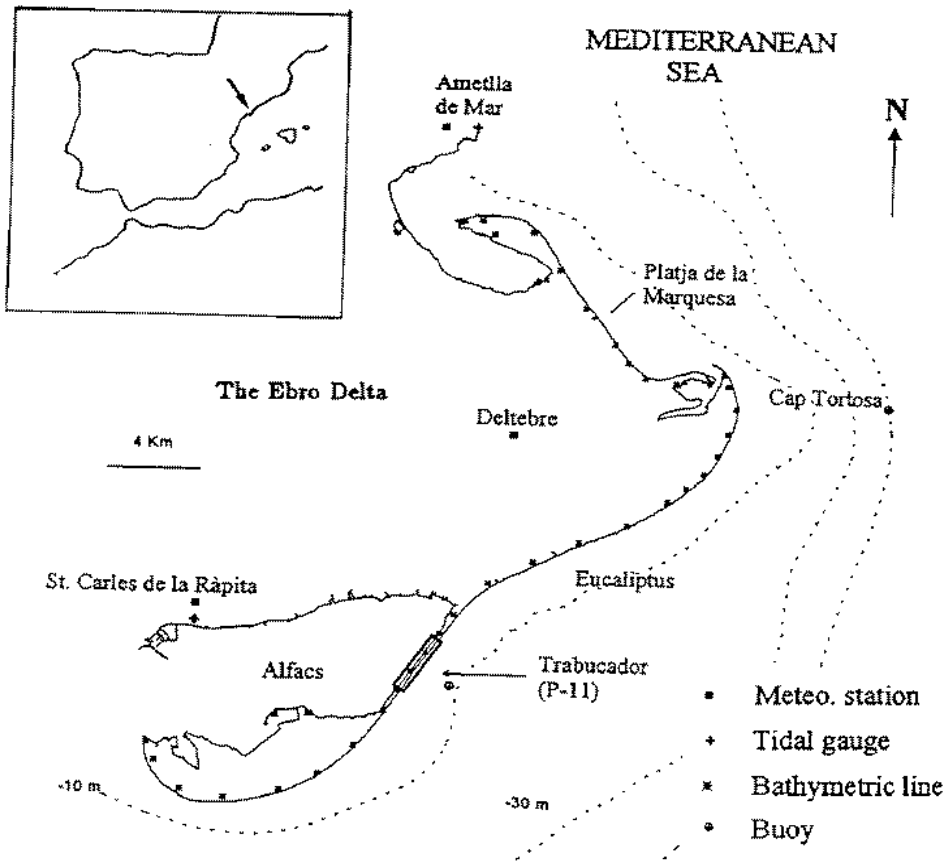


Figure 6.2: The Delta Ebro coast.

The acoustic Doppler velocimeter SONTEK-3D (ADV model Ocean) was used to measure the velocity on days 9 and 12 September, 1997, at a height of $d$=1m above the sand bottom of shallow (2 m mean depth) littoral zone in Knebel Vig

bay (figure 6.3). Knebel Vig is located at 56.3 N, 10.5 E and is a small O(3km), shallow (maximum depth 18 m) bay that is connected by a narrow channel to the larger Aarhus Bight. Thirty-minute time series of velocity were sampled at 25 Hz. The probe resolved velocities as low as 0.25 cm/s and was accurate to 0.4 cm/s and 0.1 cm/s for horizontal and vertical components, respectively. The probe mounted in a "down-looking" mode on a metal tripod and data were collected in real-time. Prior to analysis, spurious velocities were identified by low correlations (<70%) and signal strengths (5*db*) between the 3 transducer channels and edited from files.

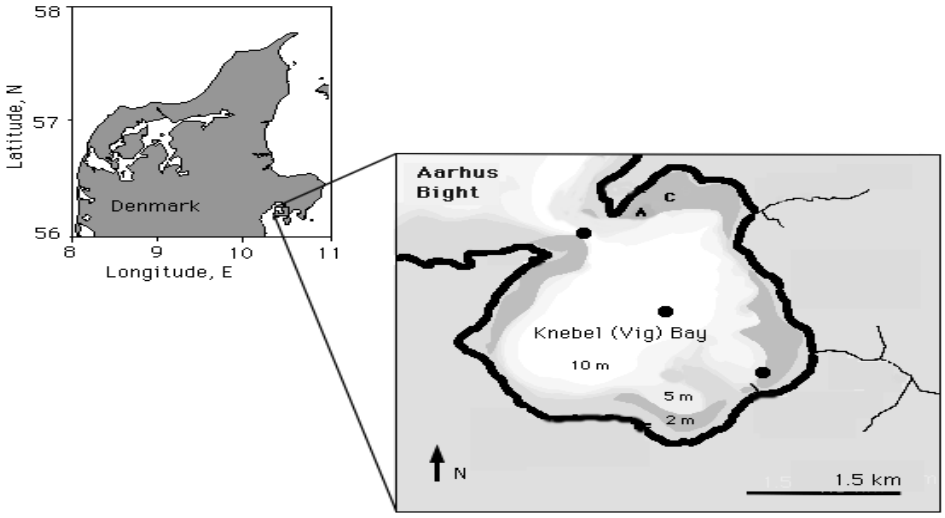


Figure 6.3: The Knebel Vig bay.

## 6.2 Absolute energy transfer

The absolute energy transfer was calculated for both Knebel Vig experiment and Delta Ebro experiment using the approximation (5.2) and the results are shown in figures 6.4 and 6.5. The figures illustrate the behavior of the absolute energy transfer $\sigma_\tau^*$ as a function of time for different time $\tau$. One can observe two different anomalies, the non-local dynamics related to the non-uniformity in scale of the energy transfer random field and the intermittency related to the largest but rarest events.

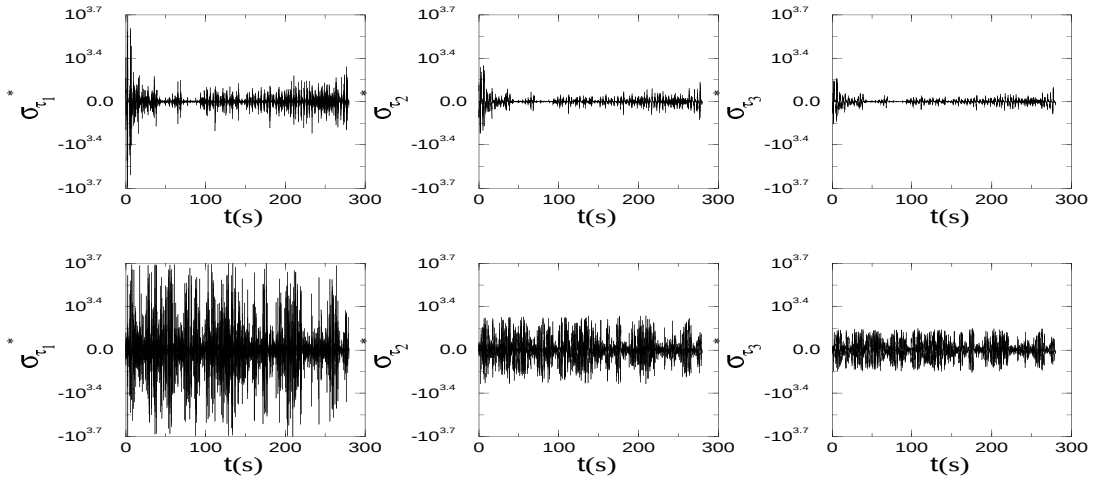


Figure 6.4: Local energy transfer $\sigma_\tau^*$ as a function of time in the Knebel Vig experiment on 9 and 12 September for three different time lags ($\tau_1 = 0.5s, \tau_2 = 1s, \tau_3 = 1.5s$).

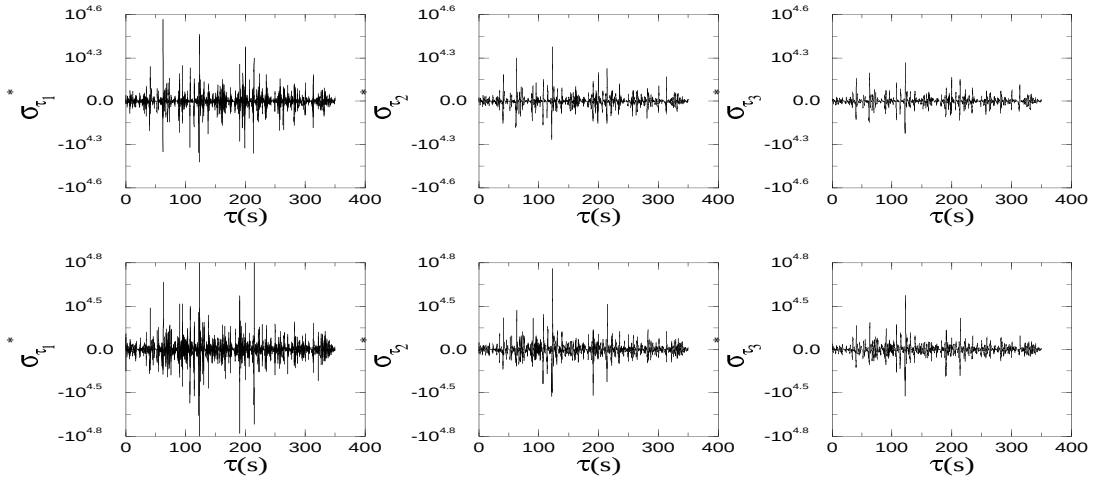


Figure 6.5: Local energy transfer $\sigma_\tau^*$ as a function of time in the Delta Ebro experiment on 27 November at non-dimensional distances from the bottom $Z/d = 0.07$ and $Z/d = 0.8$ for three different time lags ($\tau_1 = 0.4s, \tau_2 = 0.8s, \tau_3 = 1.2s$).

## 6.3 Velocity structure functions

In most geophysical flows, the velocity signal is not stationary in time and the turbulence intensity is higher, with values of $r.m.s$ velocity comparable to or larger than the mean velocity. Therefore, Taylor's hypothesis (Taylor (1938)) could not be used to convert temporal increment $\tau$ to spatial increment $\ell$ as done in the laboratory flows of chapter 5. In this case, the $pth$ order velocity structure function is defined as:

$$S_p(\tau) = \langle(\delta u(\tau)^p\rangle = \langle(u(t+\tau) - u(t))^p\rangle, \tag{6.1}$$

where $\tau$ is a time lag defining the velocity difference, the brackets $\langle..\rangle$ denote the ensemble average that is represented by an average over a certain period $t$ with the time lag $\tau$ being fixed.

More information about the structure functions was given in chapter 2, in Frisch (1995) and others (Vincent and Meneguzzi (1991), Maneveau and Sreenivasan (1991)). For data analysis, $p$ may range from 1 to 10 but this higher order requires very long time series in order to examine the statistical behavior of the structure function accurately (Gagne and Villermaux (1994)). One must be very careful in drawing any conclusions from calculations of statistical moments for $p$ higher than 10. Following Kolmogorov's theory (Kolmogorov (1941)), the self-similarity of the velocity structure function is attained in the inertial range, which is physically defined as the range of scales in which both the forcing and the dissipation process are irrelevant. A general expression of the $p$ order structure function scaling in time can be written as:

$$\langle\delta u(\tau)^p\rangle \sim \tau^{\xi_p}, \tag{6.2}$$

where $\xi_p$ is the scaling exponent. For Kolmogorov's theory K41 (Kolmogorov (1941)), $\xi_p = p/3$. The nonlinearity of the scaling exponent with order $p$ of the statistical moment has been observed in many theoretical, experimental and numerical investigations (Antonia *et al.* (1982), She and Leveque (1994) and Sreenivasan (1997)). The departure from Kolmogorov scaling laws becomes evident for higher moment, but it is less clear for the second-order moment, which implies the Kolmogorov -5/3 power spectrum.

In fact, this violation is referred to the intermittency, when the average value of the energy dissipation $\epsilon$ is different in time and at different points in space (Frisch (1995)). Meneveau and Sreenivasan (1991) in their investigation of the atmospheric surface layer data found that the energy dissipation is extremely intermittent, and that this intermittency increases strongly with increasing Reynolds number (figure

2.3).

More information on the velocity measurements and results of their spatial variations, integral length scales and dissipation has been presented in Rodriguez *et al.* (1994) for the Ebro Delta measurements and in Mahjoub *et al.* (2000b) for the Knebel Vig measurements.

Figures 6.6 and 6.7 show the velocity structure functions as a function of time $\tau$, for $p$ ranging from 1 to 6, without using the absolute value of the velocity increments $\mid \langle \delta u(\tau)^p \rangle \mid$ as a function of temporal increment $\tau$, respectively for the Knebel Vig experiment at a fixed depth $d = 1m$ on days 9 and 12 of September and for the Delta Ebro experiment on day 27 of November at non-dimensional distances from the bottom $Z/d = 0.07$ and $Z/d = 0.8$. Figures 6.8 and 6.9 show the quantity $\langle \mid \delta u(\tau) \mid^p \rangle$ as a function of temporal increment $\tau$, respectively for the Knebel Vig experiment on days 9 and 12 of September.

Even moments $\mid \langle \delta u(\tau)^p \rangle \mid$ show good scaling with $\tau$ in both experiments. In contrast, odd moments $\mid \langle \delta u(\tau)^p \rangle \mid$ seem to be less correlated with $\tau$. By taking the absolute value of the odd moments, we can also show that $\langle \mid \delta u(\tau) \mid^p \rangle$ has a monotonous increasing behavior on $p$. It can be seen that the scaling properties of the two quantities for both experiments are increasingly different and this difference becomes larger by increasing $p$. These results are consistent with non-homogeneous and non-isotropic flow measurements in the numerical research (Babiano *et al.* (1995, 1997)) and in laboratory measurements (Mahjoub *et al.* (1998)). To clarify this behavior we have also plotted the ratio $R = \langle \delta u(\tau)^3 \rangle / \langle \mid \delta u(\tau) \mid^3 \rangle$ as a function of time $\tau$ for the Knebel Vig experiment and for the Delta Ebro experiment. The results are shown in figures 6.10 and 6.11. The scaling properties of the two quantities differ increasingly.

This fact, indicates that the choice of the absolute values of the velocity differences in geophysical flows is necessary in order to study the non-homogeneous turbulent dynamics. Therefore, we define hereafter the velocity structure functions with an absolute value:

$$\langle \mid \delta u(\tau) \mid^p \rangle \sim \tau^{\zeta_p}, \tag{6.3}$$

where $\zeta_p$ is the absolute scaling exponent, which may be different from the scaling exponent $\xi_p$ for odd values of $p$.

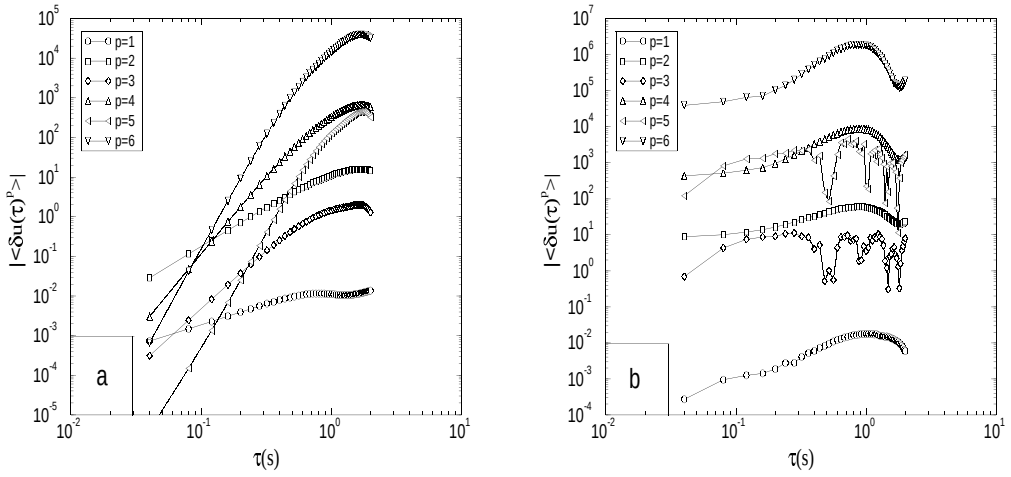


Figure 6.6: The velocity structure functions $|\langle \delta u(\tau)^p \rangle|$ as a function of time $\tau$ for the Knebel experiment on 9 September ($a$) and 12 September ($b$).

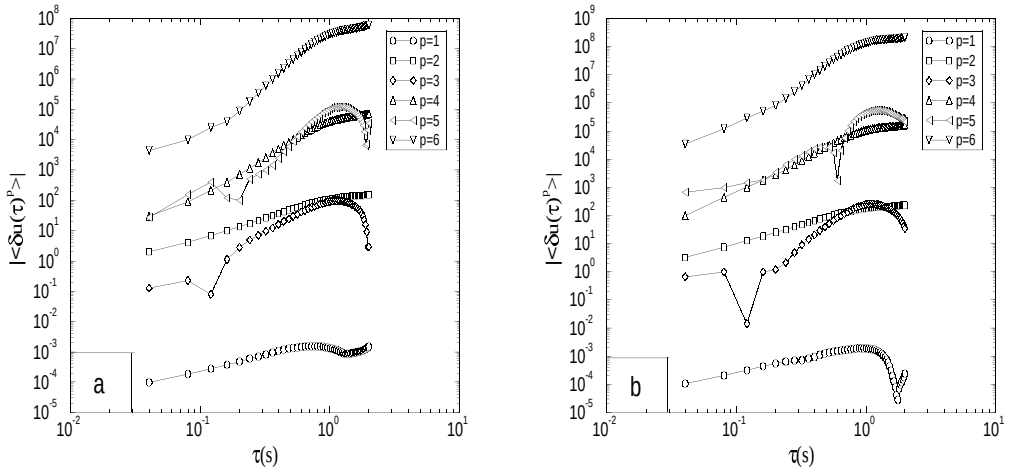


Figure 6.7: The velocity structure functions $|\langle \delta u(\tau)^p \rangle|$ as a function of time $\tau$ for the Delta Ebro experiment on 27 November at depths $Z/d = 0.07$ ($a$) and $Z/d = 0.8$ ($b$).

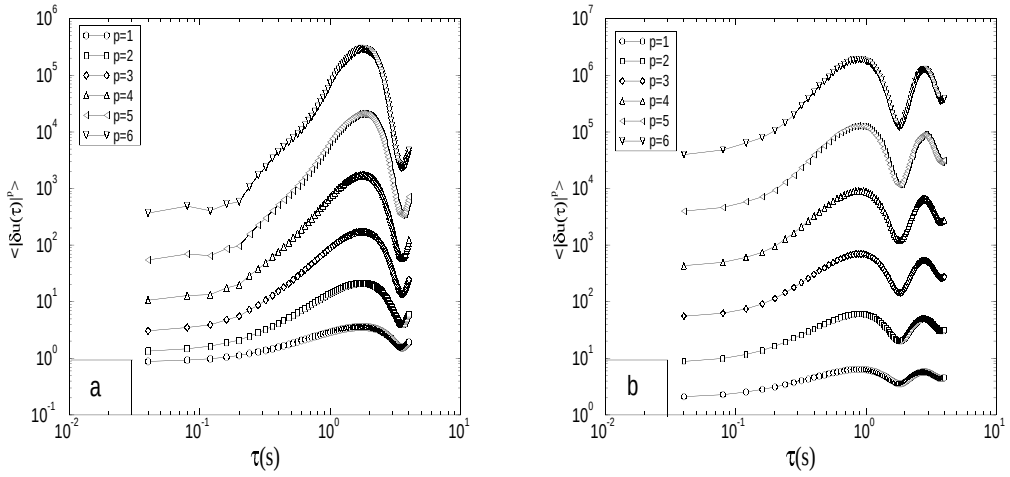


Figure 6.8: The velocity structure functions $\langle \mid \delta u(\tau) \mid^p \rangle$ as a function of time $\tau$ for the Knebel experiment on 9 September ($a$) and 12 September ($b$).

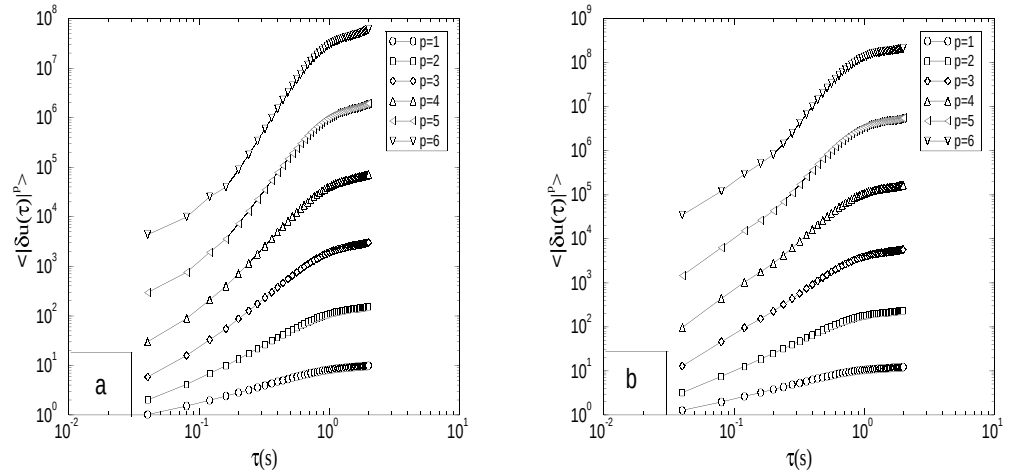


Figure 6.9: The velocity structure functions $\langle \mid \delta u(\tau) \mid^p \rangle$ as a function of time $\tau$ for the Delta Ebro experiment on 27 November at non-dimensional distances from the bottom $Z/d = 0.07$ ($a$) and $Z/d = 0.8$ ($b$).

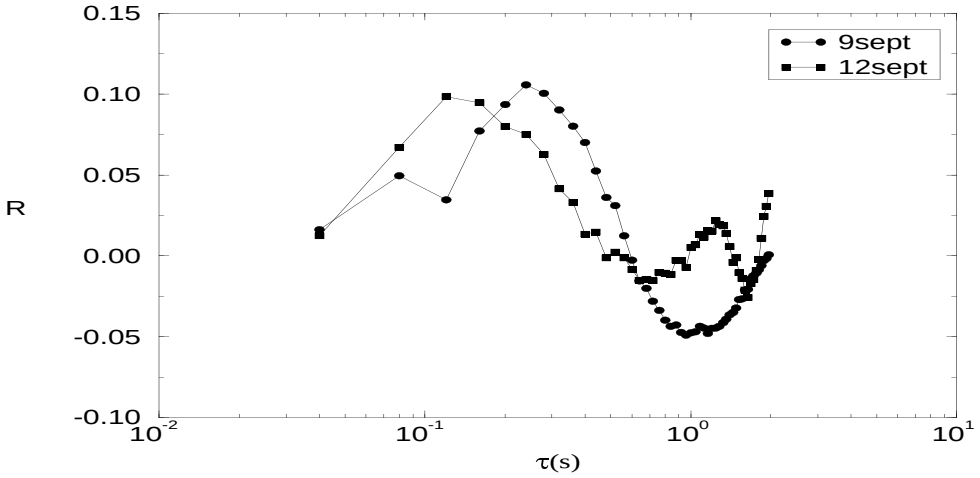


Figure 6.10: The ratio $R = \langle \delta u(\tau)^3 \rangle / \langle \mid \delta u(\tau) \mid^3 \rangle$ as a function of time in the Knebel Vig experiment on 9 and 12 September.

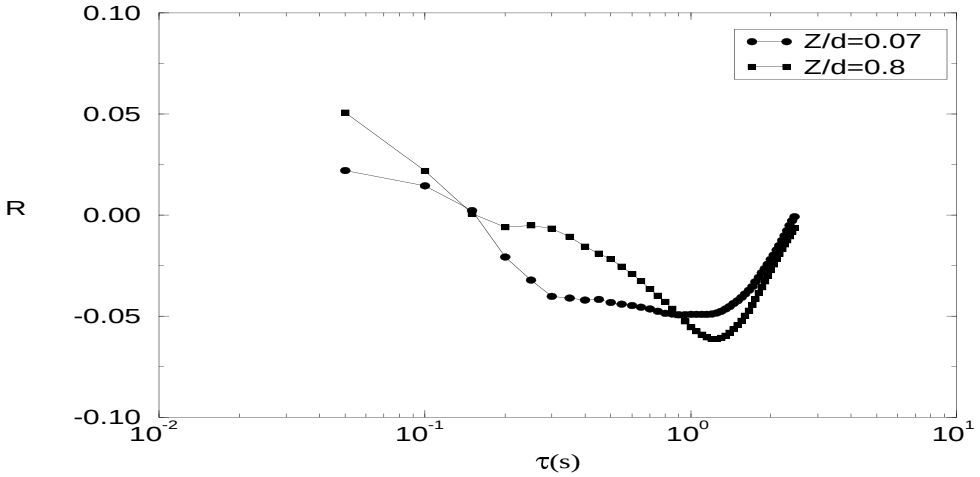


Figure 6.11: The ratio $R = \langle \delta u(\tau)^3 \rangle / \langle \mid \delta u(\tau) \mid^3 \rangle$ as a function of time in the Delta Ebro experiment on 27 November at non-dimensional distances from the bottom $Z/d = 0.07$ and $Z/d = 0.8$.

## 6.4 The absolute scaling exponent $\zeta_p$

It is usually very difficult to obtain a statistical estimation of the absolute scaling exponent $\zeta_p$ in geophysical flows even at large Reynolds numbers, because no inertial range is detected when plotting $\zeta_p$ versus the temporal increment $\tau$. This behavior is also present in homogeneous flows at low and moderate Reynolds numbers (Camussi and Guj (1996)). The inertial range is usually done by plotting $\langle \mid \delta u(\tau) \mid^3 \rangle$ versus $\tau$, where the third-order absolute scaling exponent $\zeta_3$ should be 1 (Kolmogorov (1941)). In geophysical flows, which are usually non-homogeneous and non-isotropic, this methodology cannot always be applied because the absolute scaling exponent cannot be scale independent. This aspect is clearly shown in figures 6.8 and 6.9 for Knebel Vig experiment on 9 September and 12 September and for Delta Ebro experiment on day 27 of November at non-dimensional distances from the bottom $Z/d = 0.07$ and $Z/d = 0.8$. It is clearly shown that there is no inertial range where the slope of the third-order velocity structure function $\langle \mid \delta u(\tau) \mid^3 \rangle$ is equal to 1. Model calculation and theories which assume homogeneity and isotropy will not work well in these situations.

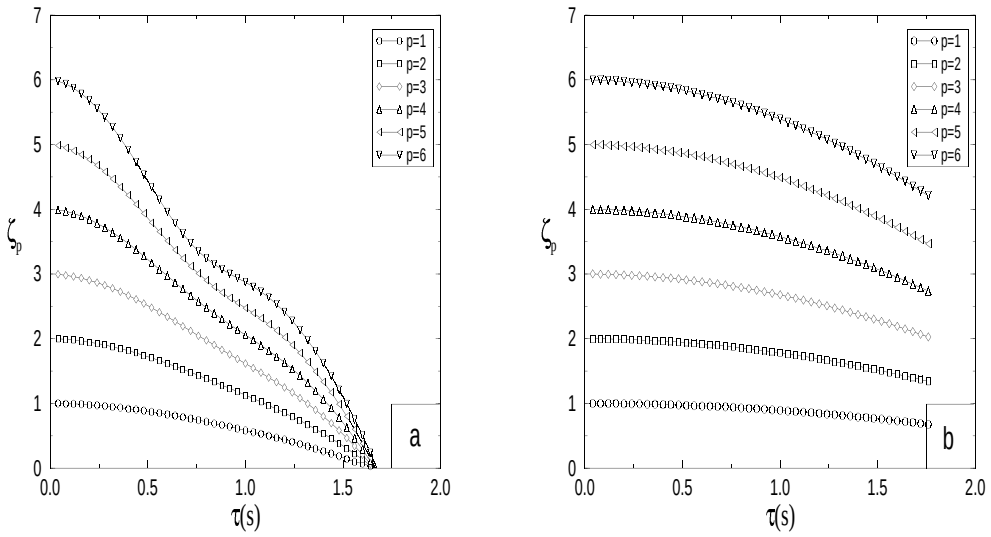


Figure 6.12: The absolute scaling exponents $\zeta_p$, as a function of time $\tau$ for the Knebel experiment on 9 September ($a$) and 12 September ($b$).

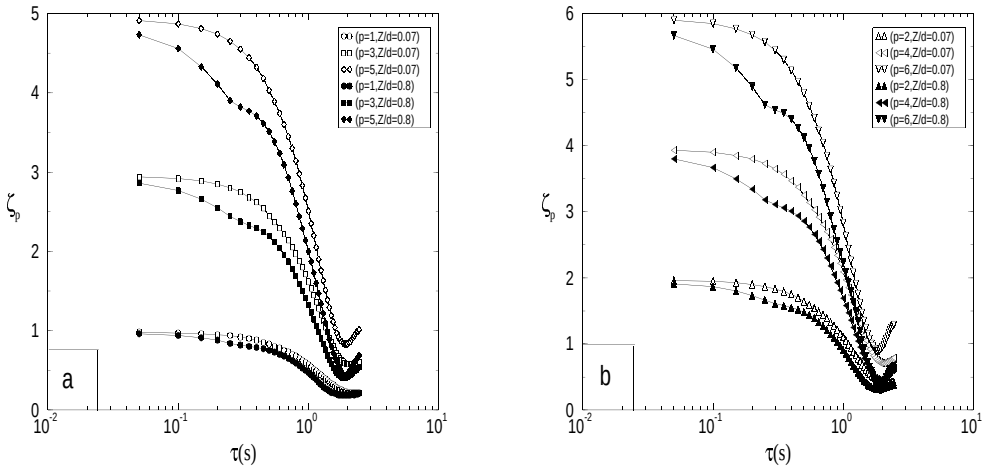


Figure 6.13: The absolute scaling exponents $\zeta_p$, as a function of time $\tau$ for the Delta Ebro experiment on 27 November at non-dimensional distances from the bottom $Z/d = 0.07$ and $Z/d = 0.8$ for odd $p$ ($a$) and even $p$ ($b$).

To clarify this behavior, figures 6.12 and 6.13 show the absolute scaling exponent $\zeta_p$ as a function of $\tau$ for the same experiments. $\zeta_p$ is strongly dependent on $\tau$ for both experiments and there is no range where $\zeta_p$ is scale independent.

This observation that in strongly non-homogeneous flows the third-order structure function is not unity was also found in the laboratory experiments reported in chapter 5 and agrees with the two dimensional numerical simulation of non-homogeneous turbulence by Babiano *et al.* (1995, 1997) and with the experimental results of three dimensional non-homogeneous turbulence by Mahjoub *et al.* (1998). These results suggest that the inertial range and the scaling laws of the velocity structure functions in geophysical flows cannot be detected simply according to the phenomenological theories suggested by (Kolmogorov (1941, 1962)), even at very high Reynolds numbers.

## 6.5 The relative scaling exponents $\zeta_p/\zeta_3$

To overcome the difficulties in determining the scaling exponent, we have used the Extended Self Similarity (ESS) technique, described in chapter 3. This method was effective in determining accurate scaling exponents in geophysical flows where there

is a deviation from local homogeneity and isotropy. Moreover, the existence of ESS could be a straightforward way to define an inertial range in these flows, where the phenomenological theories suggested by Kolmogorov (1941, 1962) do not work. This technique was applied with success in geophysical flows (Babiano *et al.* (1995, 1997) and Mahjoub *et al.* (1998)) and in magneto-hydrodynamic (MHD) turbulence (Marsch and Liu (1993), Carbone (1994, 1996), Potitano and Pouquet (1998)).

As with the laboratory data the relative scaling exponents have been calculated using the relation:

$$\langle \mid \delta u(\tau) \mid^p \rangle \sim \langle \mid \delta u(\tau) \mid^3 \rangle^{\zeta_p/\zeta_3}, \tag{6.4}$$

where $\zeta_p/\zeta_3$ is the relative scaling exponent. Equivalently,

$$\zeta_p/\zeta_3 = \frac{dlog\langle \mid \delta u(\tau) \mid^p \rangle}{dlog\langle \mid \delta u(\tau) \mid^3 \rangle}. \tag{6.5}$$

Comparisons of measured relative scaling exponents on days 9 and 12 of September in Knebel Vig experiment, and on day 27 of November at depths $Z/d = 0.07$ and $Z/d = 0.8$ in Delta Ebro experiment are shown in figures 6.14 and 6.15 respectively. In the Knebel Vig experiment the relative scaling exponents $\zeta_p/\zeta_3$ are obtained by a linear best fitting of $log\langle \mid \delta u(\tau) \mid^p \rangle$ versus $log\langle \mid \delta u(\tau) \mid^3 \rangle$, while in the Delta Ebro experiment, the relative scaling exponents $\zeta_p/\zeta_3$ are obtained using equation (6.5). As can be seen the two methods of calculating the relative scaling exponents work very well.

For both experiments the ESS technique works satisfactorily. The departure from the linear law K41 (Kolmogorov (1941)) is observed for both experiments. On the other hand, the values of $\zeta_p/\zeta_3$ on 12 September in the Knebel experiment were more intermittent than on 9 September due to the greater amplitude of the waves on 12 September. The same behavior was observed in the Delta Ebro experiment where $\zeta_p/\zeta_3$ was more intermittent at $Z/d = 0.8$ than at $Z/d = 0.07$, indicating the influence of the breaking waves on the scaling laws. One can also see that at both depths the $\zeta_p/\zeta_3$ do not depend on the temporal increment $\tau$.

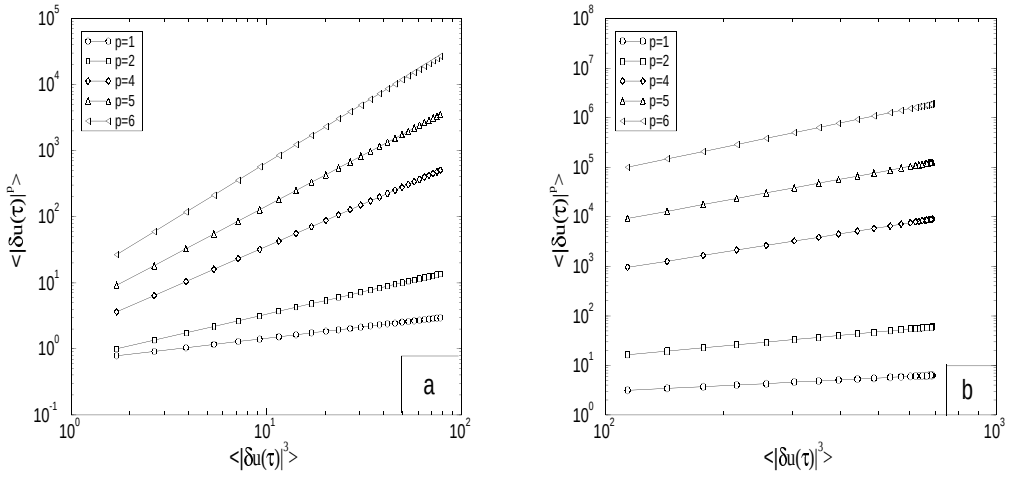


Figure 6.14: $\langle \mid \delta u(\tau) \mid^p \rangle$ as a function of $\langle \mid \delta u(\tau) \mid^3 \rangle$ for Knebel experiment on 9 September ($a$) and 12 September ($b$).

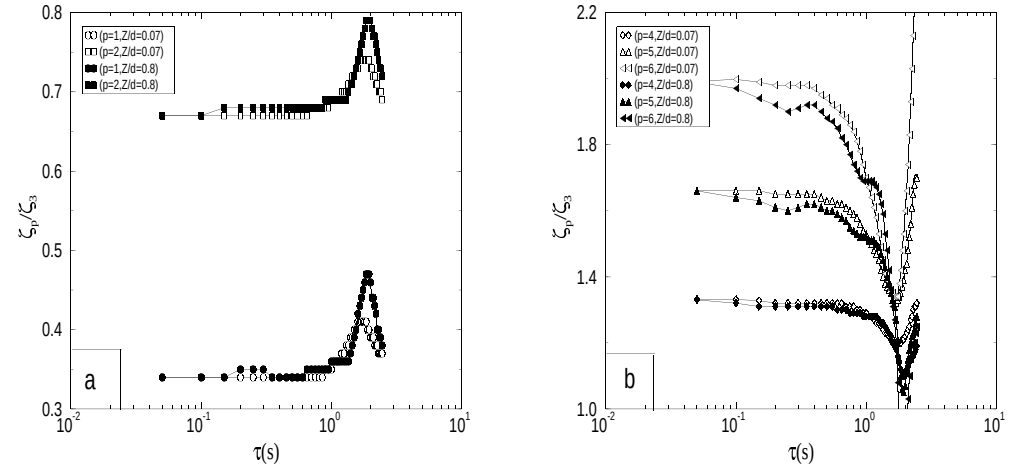


Figure 6.15: The relative scaling exponents $\zeta_p/\zeta_3$ as a function of time $\tau$ for Delta Ebro experiment on 27 November at non-dimensional distances from the bottom $Z/d = 0.07$ ($a$) and $Z/d = 0.8$ ($b$) for $p = 1, 2$ ($a$) and $p = 4, 5, 6$ ($b$).

The non-universality of the relative scaling exponents $\zeta_p/\zeta_3$ seem to be affected by the strong non-homogeneity of the turbulent flow induced by high wave motions and by the breaking waves. These results are in agreement with the laboratory experiments, which show that $\zeta_p/\zeta_3$ in non-homogeneous and non isotropic flows may not be universal.

In table 6.1 we present the values of the relative scaling exponents for both the Delta Ebro and Knebel Vig experiments; we also include the theoretical prediction of Kolmogorov (K41). It is clearly shown that all results differ from Kolmogorov's prediction (K41) and have different values. In the Delta Ebro experiment, the relative scaling exponents weremore intermittent at $Z/d = 0.8$ than at $Z/d = 0.07$, which demonstrates the influence of breaking waves on the surf-zone. In the Knebel Vig experiment, the relative scaling exponents were more intermittent on 12 September than on 9 September due to the higher wave motions on 12 September.

| *p* | *K41* | *(Z/d=0.07)* | *(Z/d=0.8)* | *9 of September* | *12 of September* |
|---|---|---|---|---|---|
| *2* | *0.66* | *0.71* | *0.69* | *0.76* | *0.71* |
| *4* | *1.33* | *1.25* | *1.27* | *1.19* | *1.26* |
| *5* | *1.66* | *1.46* | *1.48* | *1.35* | *1.48* |
| *6* | *2.00* | *1.63* | *1.66* | *1.49* | *1.67* |

Table 6.1: Comparison of the measured relative scaling exponents of both the Delta Ebro and Knebel Vig experiments with respect to the Kolmogorov theory (K41).

## 6.6 Intermittency parameters $\mu$ and $\beta$

Figure 6.16 illustrates the behaviour of $\mu$ as a function of the depths $Z/d$ in the Delta Ebro experiment. $\mu$ is clearly dependent on the depth $Z/d$ from the sea bottom. This result agrees with the results of relative scaling exponents. Due to the short time series data we have not calculated the hierarchy transfer, but we have estimated the intermittency parameter $\beta$ taking a constant value of $\Delta = 2/3$ (see Babiano (2000)). Figure 6.17 shows the intermittency parameter $\beta$ as a function of non-dimensional distances from the bottom $Z/d$. It is clearly shown that $\beta$ depends on the $p$ order structure function. On the other hand, $\beta$ decreases as a function of $Z/d$. This result proves that the intermittency is not distributed uniformly in non-homogeneous flows; there are regions with more intermittency near the surface and regions with less intermittency near the sea bottom.

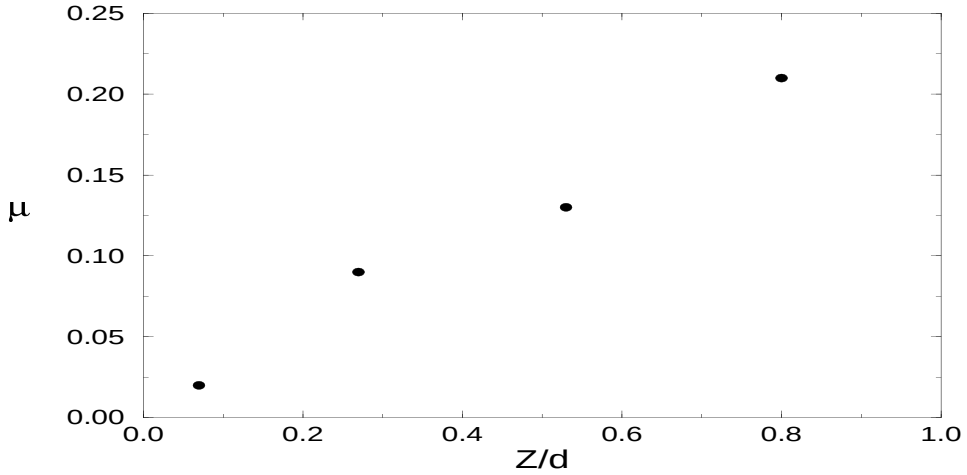


Figure 6.16: The intermittency parameter $\mu$ as a function of non-dimensional distances from the bottom $Z/d$ in the Delta Ebro experiment on 27 November.

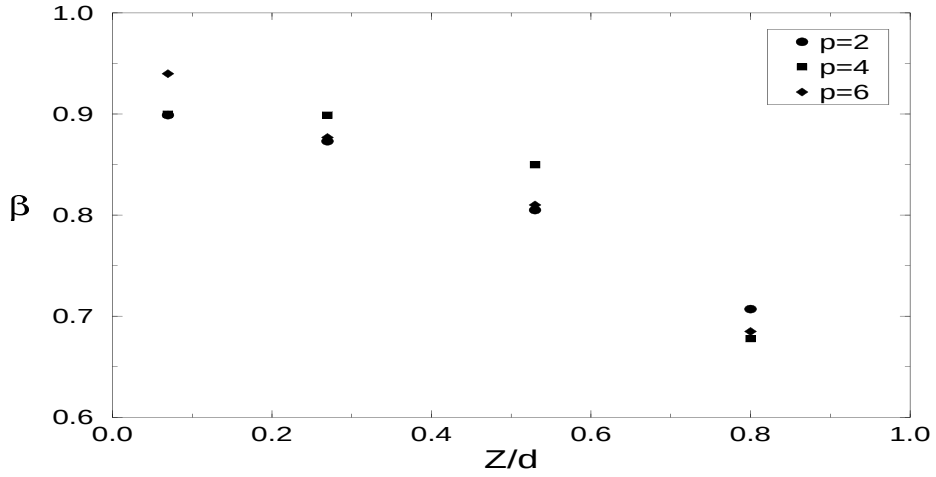


Figure 6.17: The intermittency parameter $\beta$ as a function of non-dimensional distances from the bottom $Z/d$ in the Delta Ebro experiment on 27 November.

## 6.7 Energy Spectrum

The behavior of the energy spectrum $E(f)$ was also analyzed in Fourier space. The energy spectrum was computed using a Fast Fourier Transform. The spectral process was performed with 128 blocks of 256 points and averaging the spectral densities to obtain the prototype spectrum E(f) for the respective turbulence conditions. Figure 6.18 shows the energy spectra for days 9 and 12 of September 1997 in the Knebel Vig bay experiment, while figure 6.19 shows the energy spectra for day 27 of November 1996 at non-dimensional distances from the bottom $Z/d = 0.8$ and $Z/d = 0.07$ in the Delta Ebro experiment. In the Knebel vig bay experiment, the amplitude energy of day 12 of September was higher than on day 9 of September as a result of higher and faster wind generated wave activity on day 12.

The behavior observed in the Delta Ebro experiment on day 27 of November shows that the amplitude of the waves was much smaller. It may also be seen that the energy at $Z/d = 0.8$ is higher than at $Z/d = 0.07$ as a result of the breaking waves in the surf-zone.

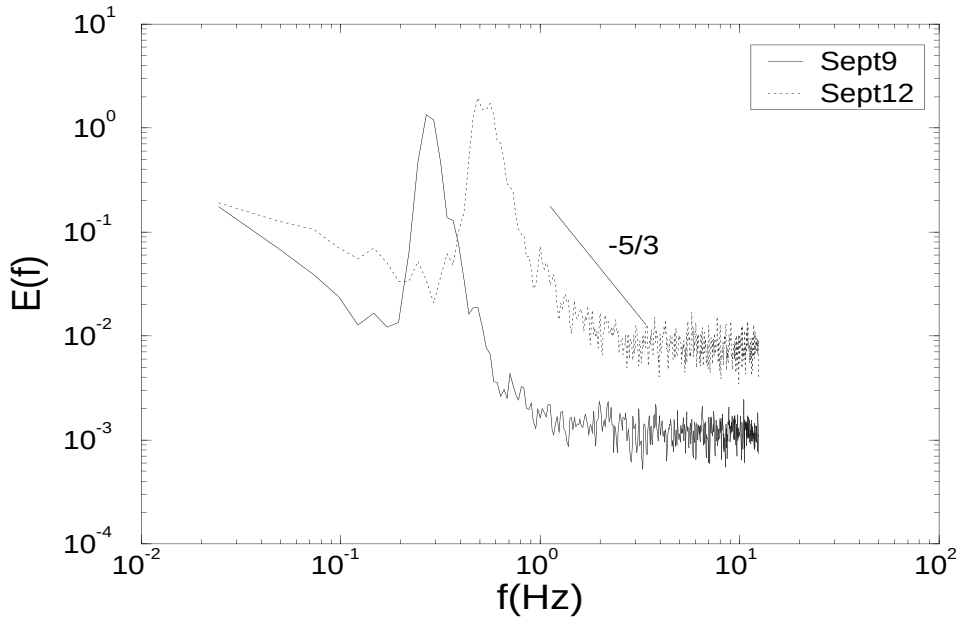


Figure 6.18: The energy spectrum as a function of frequency $f$ for the Knebel Vig bay experiment on 9 September and 12 September.

In both experiments, it should be noted that the energy spectrum is independent of the frequency $f$ in the inertial range. This mean that the Fourier transform does not imply identical span of the power law range. The predicted universal $f^{-5/3}$ frequency dependence of turbulent spectral densities is observed in both experiments. However, this does not mean that the flow in these experiments is homogeneous and non-intermittent, but this is due to the fact that the deviation from the Kolmogorov theory K41 for the low order moments is small. Consequently, this confirms that the use of the velocity structure function is a sensitive tool to understand the complex dynamic of the geophysical flows, and that higher order moment information is much more useful than the spectra.

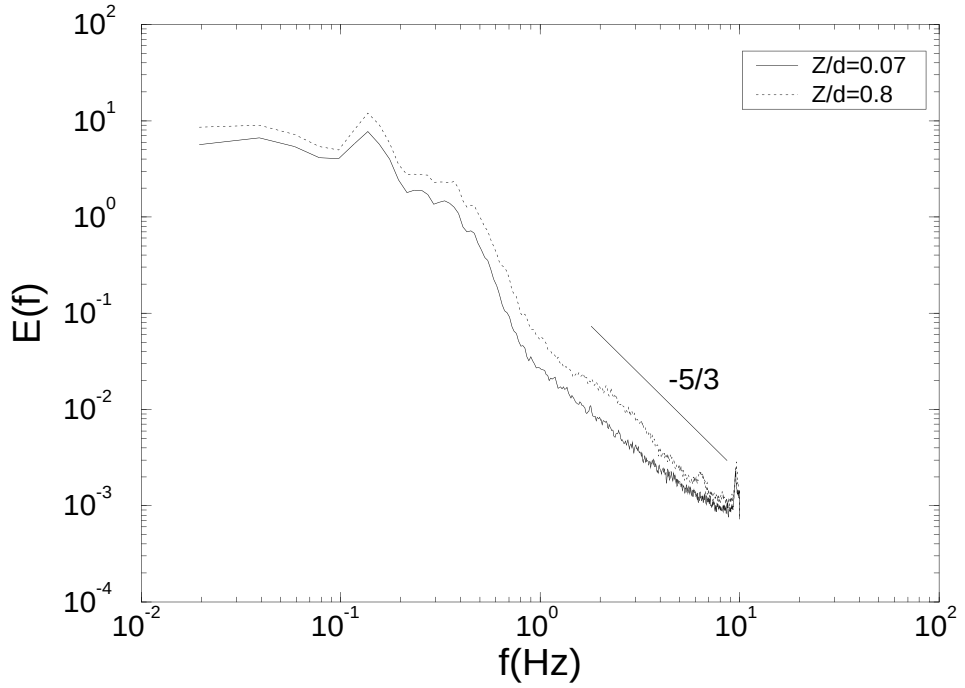


Figure 6.19: The energy spectrum as a function of frequency $f$ for the Delta Ebro experiment on 27 November at non-dimensional distances from the bottom $Z/d = 0.07$ and $Z/d = 0.8$.

## 6.8 Probability distribution functions (PDF)

The PDF of geophysical data has recently received much attention as well as the power spectra and the structure functions. Instead of just using the structure function of the velocity differences, one can also study the probability distributions of the velocity difference $\delta u(\tau) = u(t+\tau) - u(t)$ and analyze their shapes. The PDFs are often plotted logarithmically versus $\delta u(\tau)$. Recently, Weiss *et al.* (1998) and Bracco *et al.* (1999), in their analysis using a large number of subsurface float trajectories in the ocean found that the velocity PDFs are not Gaussian but nearly exponential wings and they concluded that the deviation from a Gaussian distribution is the result of non-uniform deployments, because the ocean is so inhomogeneous. The PDFs of the velocity fluctuations presented here are normalized, i.e., the random variable on the abscissa is equal to $\Delta u = \frac{(u(t)-U_0)}{rms(u(t)-U_0)}$, and the ordinate value $P(\Delta u)$ is such that the area under the PDF curve is equal to one.

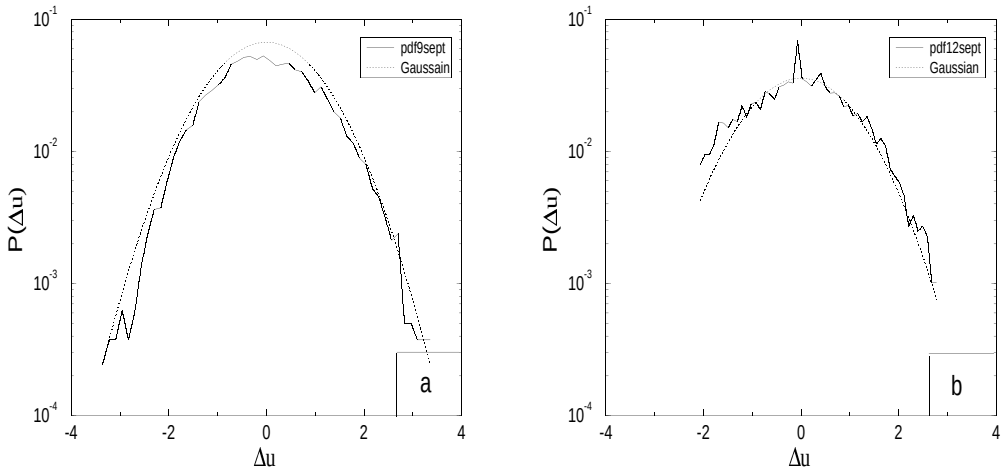


Figure 6.20: The Probability distribution function for the Knebel Vig bay experiment on 9 September and 12 September.

Figures 6.20 and 6.21 show the probability distribution functions of the normalized density fluctuations for 9 September and 12 September in the Knebel Vig experiment and for 27 November at non-dimensional distances from the bottom $Z/d = 0.8$ and $Z/d = 0.07$ in the Delta Ebro experiment. For comparison, the dotted lines show the Gaussian distribution. In all the curves deviation from Gaussian distribution is observed. In the Knebel Vig bay experiment this deviation is

greater on 12 September than on 9 September. This anomalous behavior, especially on 12 September is related as discussed above and in Mahjoub *et al.* (2000b) to the strong wind, which was more energetic than on 9 September (figure 6.18). The same type of behavior is also observed in Delta Ebro experiment, which show that the deviation from Gaussian behavior is more pronounced at $Z/d = 0.8$ near the surface at large velocity fluctuations than at $Z/d = 0.07$ due to the breaking waves. These results agree with the non-homogeneous character of turbulence discussed in previous chapters.

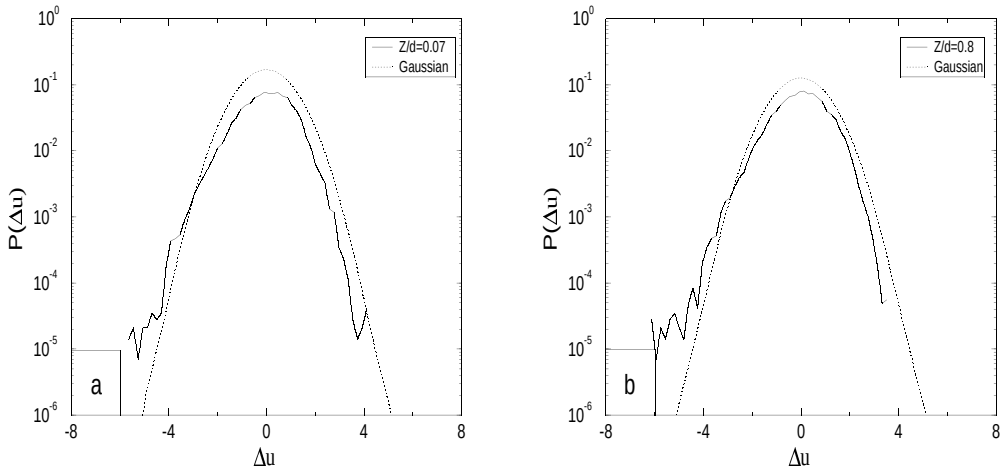


Figure 6.21: The probability distribution function for Delta Ebro experiment on 27 November at non-dimensional distances from the bottom $Z/d = 0.07$ and $Z/d = 0.8$.